Available online at www.eccomasproceedia.org
Eccomas Proceedia COMPDYN (2025) 1201-1210

ECCOMAS
Proceedia

COMPDYN 2025
10th ECCOMAS Thematic Conference on
Computational Methods in Structural Dynamics and Earthquake Engineering
M. Papadrakakis, M. Fragiadakis (eds.)
Rhodes Island, Greece, 15-18 June 2025

EXPERIMENTAL CAMPAIGN OF THE RATE-INDEPENDENT PRESSURIZED SAND DAMPERS

Konstantinos N. Kalfas[1], Nicos Makris[2]

[1] The University of Texas at Tyler
Dept. of Civil and Construction Engineering and Management, Tyler, TX 75799
e-mail: kkalfas@uttyler.edu

[2] Southern Methodist University
Dept. of Civil and Environmental Engineering, Dallas, TX 75205
nmakris@smu.edu

Abstract

This study presents results from cyclic testing on various configurations of a recently developed pressurized sand damper (PSD) in which a steel sphere is moving within a cylindrical tube filled with sand that is under pressure. The experimental campaign investigated the effects of the key design parameters of the damper, namely, the effect of the clearance between the moving sphere and the cylindrical tube and the effect of the overall length of the damper to its force output. The recorded force–displacement loops when normalized to the strength of the pressurized sand damper reveal remarkable order with stable behavior and confirm that the force output is nearly rate-independent.

Keywords: Pressurized Sand Damper, Rate-Independent, Hysteretic Behavior, Energy Dissipation; Response-Modification Devices, Granular Materials.

ISSN:2623-3347 © 2025 The Authors. Published by Eccomas Proceedia.
Peer-review under responsibility of the organizing committee of COMPDYN 2025.
doi: 10.7712/120125.12483.25481

1 INTRODUCTION

Earthquakes, winds and traffic loading on bridges, induce vibrations of different amplitudes and durations, yet detrimental. Earthquakes for example induce large structural displacements and velocities with a finite duration, whereas the prolonged winds require high energy dissipation, while the traffic loading small amplitude is characterized by very long duration that may fatigue supplemental dampers and eventually lead to catastrophic failures [1]. The suppression of large earthquake-induced displacements requires long-stroke dampers; whereas the high-velocity demands that often originate from pulse-like near-source ground motions [2-4] have challenged the damping device industry to manufacture dampers with behavior that is nearly velocity-independent.

To that end, seismic isolation systems, specially designed energy dissipation devices, response-modification techniques and coupling systems that dissipate energy have been developed, to cover the increasing needs of civil structures to meet acceptable performance levels when subjected to earthquake or wind excitations. Such devices and systems which constitute alternative strategies to the traditional seismic capacity design of structures include the elastomeric bearings [5-9], fluid and hysteretic dampers [10-14], buckling-restrained braces (BRBs) [15], yielding steel dampers [16-18], tuned mass dampers (TMDs) [19], inerters [20, 21], as well as the rocking isolated systems or those coupled with fluid or hysteretic damping devices, or with inerters [22-25], among others. This study proposes a new device which is not vulnerable to failures of the end seals, while at the same time can accommodate small- and large-stroke amplitudes.

This research is partly motivated by the need to develop sustainable energy dissipation devices that do not suffer from oil leakage due to failure of their end seals [1] and from the occasional displacement limitations of the BRBs and the yielding steel dampers; and partly from the need to develop a robust damper that consists only of traditional civil engineering materials (sand and steel) in association with the use of post -tensioned steel rods with which practitioner civil engineers are familiar. Past failures of fluid dampers are both disruptive and costly, therefore not in-line with the current design paradigm of sustainable engineering, where the design and construction of structural systems shall meet acceptable performance levels at present and in the years to come without compromising the ability of future generations to use, maintain, and benefit from them.

This study presents results from extensive cyclic testing of various configurations of the proposed PSD [26-35] which does not suffer from the challenges of viscous heating, or from limited displacement capabilities and addresses the quest for velocity-independent (hysteretic) dissipation. This paper builds on previous studies [26, 29, 30, 33] and discusses the concept, design, and experimental campaign of the sustainable, innovative, cost -effective, long-stroke, fail-safe PSD, where the moving piston-rod that is enclosed within the damper housing is surrounded by pressurized sand. The limited dependence of the energy dissipation of granular materials to temperature renders the sand as an ideal dissipative material [36]. The proposed device is simple, robust in harsh environments with either high or low temperatures and delivers a stable force-displacement behavior over a large number of cycles.

2 CONCEPTION OF THE PSD, CONFIGURATIONS AND EXPERIMENTAL SETUP

2.1 Conception of the PSD

The development of the PSD is based on enclosed pressurized sand in a steel tube. This enclosed sand cannot be considered as a 'fragile material', due to the appreciable externally

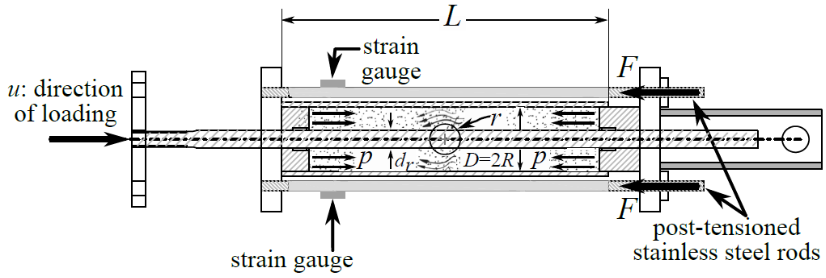

Figure 1: Schematic of the proposed PSD. The pressure applied to the enclosed sand is illustrated through a diagram of forces.

applied pressure, p, that results in a dominant hydrostatic stress tensor. The pressurized sand can be better characterized as a yielding continuum, where the drag force applied to the moving sphere is the result of the development of normal (passive) and shear stresses along the sand-steel interface.

Figure 1 shows the proposed PSD with a cylindrical damper housing of internal diameter D and length L, where a steel sphere of radius r is mounted on a double-ended piston-rod of diameter d_r. Energy is dissipated from the shearing action of the sand as the sphere mounted on the damper-piston is plowing through the pressurized sand. The pressure on the sand is exerted with external post-tensioned steel rods, where their tensile force can be monitored in real-time with strain gauges. Because of the finite length and diameter of the damper housing, the resisting force applied to the steel sphere depends on the displacement of the sphere (stroke of the damper), u, and the clearance (gap) between the steel sphere and the cylindrical tube, $D - 2r$. By following the reasoning presented in [26, 29, 30, 33] that is rooted in dimensional analysis, the resisting (drag) force, F_{SD}, on the sphere moving along the axis of the cylindrical damper housing of diameter D is expressed by:

$$F_{SD}\,(u(t)) = \Pi_S\, p\, r^2\, \varphi(u(t), r/R) + \mu\, k\, p\, \pi\, d_{rod}\, L_{net}\, \psi(u(t)) \tag{1}$$

The first term accounts for the resistance from the sphere, while the second term considers the resistance from the piston-rod due to friction., Π_S is a dimensionless coefficient that accounts for several geometric, material and loading parameters; $p= 4F/\pi D^2$ is the average pressure exerted to the sand; r is the radius of the mounted sphere on the piston-rod; $\varphi(u(t), r/R)$ is a dimensionless function that depends on the stroke, $u(t)$, and on the normalized clearance of the moving sphere from the damper housing, (r/R); μ is a friction coefficient developed along the sand–steel interface; k is a coefficient that relates the radial pressures to the exerted axial pressure, p; $\pi\, d_{rod}\, L_{net}$ is the surface of the piston-rod that is in contact with the pressurized sand; and $\psi(u(t))$ is a dimensionless function that accounts for the dilatancy of sand as it is being sheared by the moving piston-rod [26, 29, 30, 33].It is shown in previous studies from the authors [26, 29, 30, 33] that simple linear regression analysis, of the results where only the friction force that develops along the cylindrical surface of the piston-rod $\pi\, d_{rod}\, L_{net}$ is considered, yields an average estimate of the combined parameter $\mu k= 0.016$.

2.2 Configurations of the PSD

This study builds on previous studies by the authors [26, 29, 30, 33], where the main thrust was to assess the effects of two key design parameters: (a) the clearance between the moving sphere and the damper housing (r/R); and (b) the length of the damper housing (L/R). The effects of these two design parameters were assessed experimentally and are addressed in the

	Damper Housing		Sphere
	L	D= 2R	d= 2r
No	cm	cm	cm
1			5.08
2		12.38	5.72
3			-
4			5.08
5	60.96	13.97	5.72
6			-
7			5.08
8		12.38	5.72
9			5.08
10	68.58	13.97	5.72

Table 1: PSD configurations being tested in the SMU Structures laboratory.

following sections. To investigate the influence of these two parameters on the PSD behavior, multiple configurations are designed and assembled. These configurations are consisted of damper housings (cylindrical tubes) with lengths of L= 60.96, 68.58 cm, and diameters of D= 2R= 12.38, 13.97 cm; as well as of mounted spheres on the piston-rod with two different diameters: d= 2r= 5.08, 5.715 cm. The diameter of the piston-rod is: d_r= 3.175 cm. A total of 10 different configurations are assembled, which are summarized in Table 1. More details about the complete study are available in [26, 29, 30, 33].

2.3 Experimental setup

The experimental setup in the Structures Laboratory at SMU can be seen in Fig. 2, where a 245-kN hydraulic actuator with a $\pm$ 25.4 cm stroke imposes on the attached sand damper a harmonic displacement loading, $u(t) = u_0 \sin(2\pi f_0 t)$ with amplitude u_0 and frequency f_0 at various pressure levels and different frequencies. The damper housing has been filled with dry sand of an average density of $\rho \approx$ 1,900 kg/m^3 and an aggregation gradation range of 0.6 < d_{gr} < 2 mm. Additional details can be found in [26, 29, 30, 33].

After the damper housing is filled with the dry sand, the end-cap is hand-tight, while the damper is vertical. Subsequently, the damper is mounted, along its horizontal position, on the reaction frame. Then, the damper is post-tensioned at the desired pressure by reading the axial strains on the four post-tensioned stainless steel rods measured with the commercially available weldable strain gauges. These strain gauges are permanent on the post-tensioned stainless

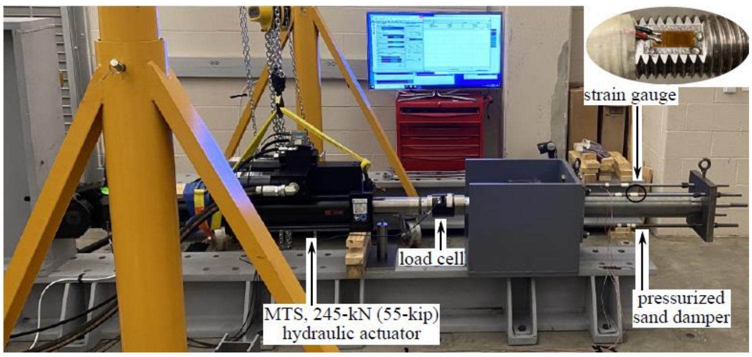

Figure 2: View of the experimental setup in the Structures Laboratory of Southern Methodist University.

steel rods to monitor over time the exerted pressure on the PSD that may need to be adjusted in the long run due to the progressive crushing of the sand grains that will happen in the neighborhood of the moving sphere after repeated cycling.

3 EXPERIMENTAL CAMPAIGN

3.1 Component testing of the PSD

Figure 3 plots selected recorded force-displacement loops from harmonic displacement loading, $u(t) = u_0\sin(2\pi f_0 t)$ with amplitude u_0 and frequency f_0, on the prototype PSDs with different sphere and damper housing diameters. Different pressure levels have been exerted (p ranges from 1 to 4 MPa), while the velocities of the piston-rod due to the applied cyclic displacements are ranging from 0.63 to 4.71 cm/sec. It is observed that the force output when the sphere is passing through the origin, which is when the sphere reaches its peak velocity during its harmonic motion, is nearly velocity-independent. The overall shape of the hysteretic loops together with the pinching behavior that manifests at larger displacements and increasing pressure levels is essentially not affected by the local behavior prior to yielding. The recorded force-displacement loops demonstrate a remarkable stable behavior of the PSD despite the 10 consecutive cycles of loading in each test.

3.2 Clearance effect between the moving sphere and the damper housing

The effect of the clearance, (r/R), on the force output is investigated experimentally by considering the configurations presented in Table 1. A total of eight different PSD configurations are considered. PSDs with two different lengths of the damper housing (L= 60.96 cm and L= 68.58 cm) and two different diameter cylinders (D= 2R= 12.38 cm and 13.97 cm). Cyclic tests are conducted by using in succession two spheres with diameters d= 2r= 5.08 cm, and 5.72 cm.

The force output from the damper during cyclic testing as the sphere mounted on the piston-rod passes by the displacement origin [u= 0 and $\varphi(0)= \psi(0)= 1$] is given by $F_{SD}(u=0) = \Pi_S\, p\, r^2 + \mu\, k\, p\, \pi\, d_{rod}\, L_{net}$. Figure 4 shows indicative plots at various pressure levels, with a

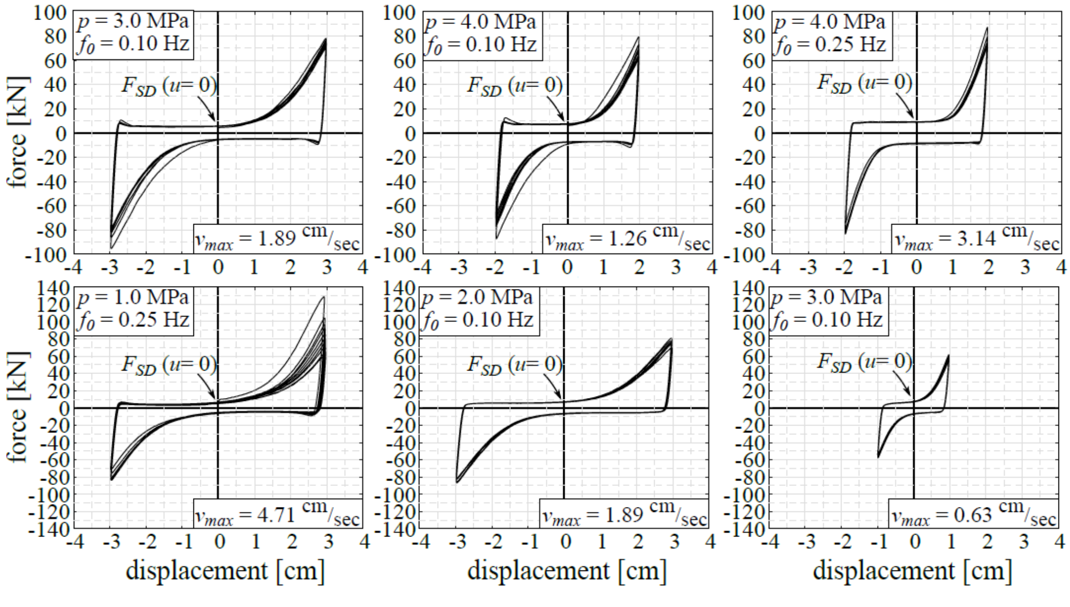

Figure 3: Recorded force-displacement loops from different PSD configurations.

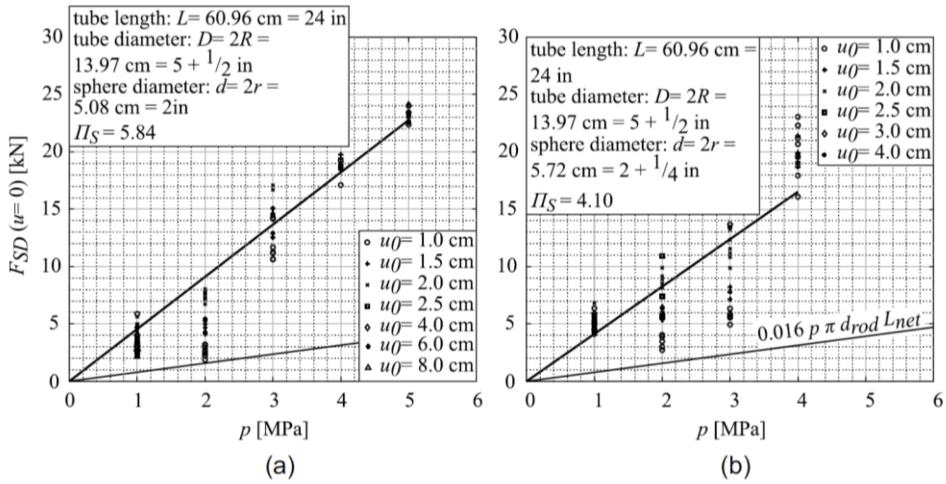

Figure 4: Measured strength, F_{SD} (u= 0), developed in the PSD during cyclic testing as the sphere passes by the displacement origin at multiple pressure levels and frequencies with two different PSD configurations.

cylinder of length L= 60.96 cm and inner diameter D= 2R= 13.97 cm. Figure 4a is when the mounted sphere has a diameter of d = 2r = 5.08 cm and the Fig. 4b is for d= 2r= 5.72 cm. The comprehensive plots of the measured strength, F_{SD} (u= 0) = $\Pi_S\, p\, r^2 + \mu\, k\, p\, \pi\, d_{rod}\, L_{net}$ of the different PSD configurations under consideration can be found in [26, 29, 30, 33].

From Equation (1), the dimensionless coefficient, Π_S, of the force output of the damper due to the sphere alone, when the sphere mounted on the piston-rod passes by the displacement origin [u= 0 and $\varphi(0)= \psi(0)= 1$], is:

$$\Pi_S = F_{SD}\,(u=0)/(p\, r^2) - \mu\, k\, \pi\, (d_{rod}\, L_{net})/r^2 \tag{2}$$

Linear regression analysis of the recorded data results in different dimensionless values of Π_S for the data shown in Fig. 4 and those presented in [26, 29, 30, 33]. The resulting values of Π_S from the four configurations with L= 60.96 cm (damper housing diameters D= 2R= 12.38 cm and 13.97 cm, and sphere diameters d= 2r= 5.08 cm, and 5.72 cm), are summarized in Fig. 5. The values of Π_S do not exhibit any trend with respect to the clearance, (r/R), suggesting that the value of Π_S is independent of the clearance, (r/R). Accordingly, this study

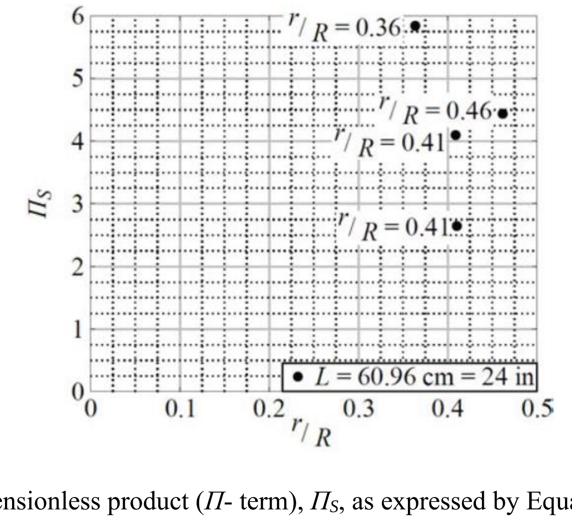

Figure 5: Values of the dimensionless product (Π- term), Π_S, as expressed by Equation (2) for the PSD with L= 60.96 cm.

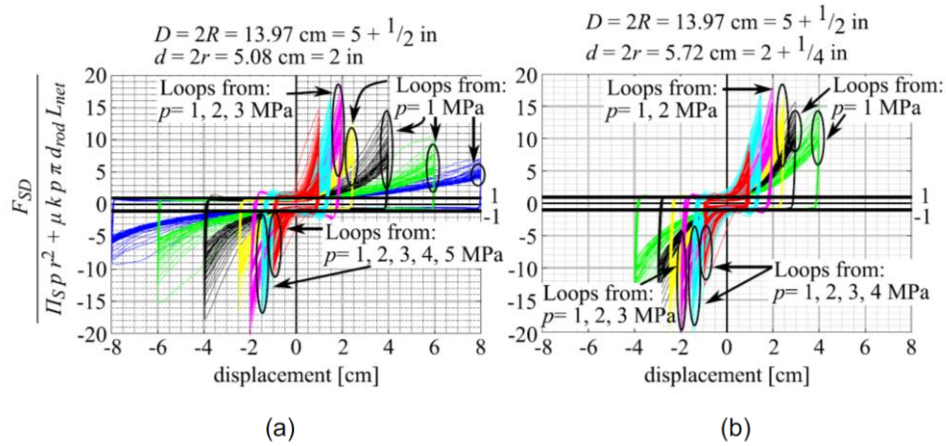

Figure 6: Recorded force-displacement loops with length L= 60.96 cm and cylinder diameter of D= 2R= 13.97 cm, at various amplitudes, exerted pressures and frequencies normalized to the average strength of the PSD, F_{SD} (u= 0) = $\Pi_S\, p\, r^2 + \mu\, k\, p\, \pi\, d_{rod}\, L_{net}$= 4.26 $p\, r^2$ + $0.016\, p\, \pi\, d_{rod}\, L_{net}$.

yields for a tube length L= 60.96 cm an average value of Π_S= (2.65 + 4.44 + 5.84 + 4.10)/4 = 4.26.

Now that an average value for the dimensionless constants Π_S= 4.26. (for the configurations with L= 60.96 cm), and an average value for the friction coefficient μk= 0.016 have been determined, Fig. 6 plots indicatively, all the force-displacement loops recorded during the experimental campaign for the two damper configurations with damper housing length L= 60.96 cm and inner diameter D= 2R= 13.97 cm (sphere diameters of d= 2r= 5.08 cm, and 5.72 cm, in Figs. 6a and 6b, respectively) shown in Fig. 4; for all frequencies and exerted pressures, normalized to the strength of the PSD, F_{SD} (u= 0) = $\Pi_S\, p\, r^2 + \mu\, k\, p\, \pi\, d_{rod}\, L_{net}$= 4.26 $p\, r^2$ + $0.016\, p\, \pi\, d_{rod}\, L_{net}$. The normalized plots exhibit remarkable order showing that the behavior of the PSD is rate-independent.

3.3 Effect of the length of the damper housing

Figure 7 plots all the resulting values of Π_S from 4 configurations with L= 60.96 cm and 4 configurations with L= 68.58 cm, as a function of (L/R). The range of (L/R) that has been

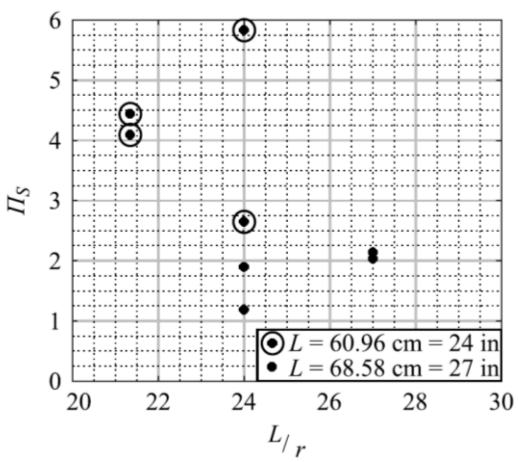

Figure 7: Values of the dimensionless product (Π- term), Π_S, as expressed by Equation 2 for the PSDs with L= 60.96 cm and L= 68.58 cm.

tested shows that there is a decreasing trend of Π_S as the (L/R) ratio increases revealing a trend that the sphere mounted on the piston-rod "feels" the finite length of the damper at the very initiation of the motion.

4 CONCLUSIONS

In this paper, part of the extensive experimental campaign, on various configurations of a recently developed PSD, in an effort to better understand the effect of the clearance between the moving sphere and the damper housing and the effect of the overall length of the damper to its force output, is presented. The presented experimental results show that the force output of the PSD at the initiation of the motion of the sphere is independent of the values of the clearance, (r/R), that were examined. These results stem from the local characteristic of the failure of the sand structure in the vicinity of the sphere. At the same time, the force output of the PSD at the initiation of motion decreases as the length of the damper cylinder increases, suggesting that the sphere “feels” the finite length of the damper even at the initiation of motion when it is at mid-stroke. When the recorded force–displacement loops for all frequencies and exerted pressures are normalized to the strength of the PSD, remarkable order emerges and confirms that the behavior of the PSD is nearly rate-independent. This work laid out an analysis framework to assess the effect of the design parameters of the PSD and can be used as a guide for the design of PSDs at different scales.

REFERENCES

[1] P. Matier, A. Ross, Bay bridge shock absorbers spring leak. *San Francisco Chronicle*, **20**, 2013.

[2] V.V. Bertero, S.A. Mahin, R.A. Herrera, Aseismic design implications of near-fault San Fernando earthquake records. *Earthquake Engineering & Structural Dynamics*, **6**(**1**), 31-42, 1978.

[3] M.F. Vassiliou, N. Makris, Estimating time scales and length scales in pulselike earthquake acceleration records with wavelet analysis. *Bulletin of the Seismological Society of America*, **101**(**2**), 596-618, 2011

[4] E. Efthymiou, N. Makris, Pulse-period─moment-magnitude relations derived with wavelet analysis and their relevance to estimate structural deformations. *Earthquake Engineering & Structural Dynamics*, **51**(**7**), 1636-1656, 2022.

[5] J.M. Kelly, *Earthquake-resistant design with rubber*. Springer, 1993.

[6] J.M. Kelly, D. Konstantinidis, *Mechanics of rubber bearings for seismic and vibration isolation*. John Wiley & Sons, 2011.

[7] K.N. Kalfas, S.A. Mitoulis, K. Katakalos, Numerical study on the response of steel-laminated elastomeric bearings subjected to variable axial loads and development of local tensile stresses, *Engineering Structures*, **134**, 346-357, 2017.

[8] K.N. Kalfas, S.A. Mitoulis, D. Konstantinidis, Influence of steel reinforcement on the performance of elastomeric bearings, *Journal of Structural Engineering*, **146**(**10**), 04020195, 2020.

[9] K.N. Kalfas, N.G. Amirabad, D. Forcellini, The role of shear modulus on the mechanical behavior of elastomeric bearings when subjected to combined axial and shear loads, *Engineering Structures,* **248**, 113248, 2021.

[10] N. Makris, Viscous heating of fluid dampers. I: Small-amplitude motions, *Journal of Engineering Mechanics*, **124**(**11**), 1210-1216, 1998.

[11] N. Makris, Y. Roussos, A.S. Whittaker, J.M. Kelly, Viscous heating of fluid dampers. II: Large-amplitude motions, *Journal of Engineering Mechanics*, **124**(**11**), 1217-1223, 1998.

[12] E. Tubaldi, M. Barbato, A. Dall'Asta, Performance-based seismic risk assessment for buildings equipped with linear and nonlinear viscous dampers, *Engineering Structures*, **78**, 90-99, 2014.

[13] L. Cao, A. Downey, S. Laflamme, D. Taylor, J. Ricles, Variable friction device for structural control based on duo-servo vehicle brake: Modeling and experimental validation, *Journal of Sound and Vibration*, **348**, 41-56, 2015.

[14] L. Cao, S. Laflamme, D. Taylor, J. Ricles, Simulations of a variable friction device for multihazard mitigation, *Journal of Structural Engineering*, **142**(**12**), H4016001, 2016.

[15] C.J. Black, N. Makris, I.D. Aiken, Component testing seismic evaluation and characterization of buckling restrained braces. *Journal of Structural Engineering*, **130**(**6**), 880-894, 2004.

[16] M. Titirla, K. Katakalos, G. Zuccaro, F. Fabbrocino, On the mechanical modeling of an innovative energy dissipation device. *Ingegneria Sismica-International Journal of Earthquake Engineering*, 126-138, 2017.

[17] M.D. Titirla, P.K. Papadopoulos, I.N. Doudoumis, Finite element modelling of an innovative passive energy dissipation device for seismic hazard mitigation. *Engineering Structures*, **168**, 218-228, 2018.

[18] M.D. Titirla, A state-of-the-art review of passive energy dissipation systems in steel braces. *Buildings*, **13**(**4**), 851, 2023.

[19] L. Marian, A. Giaralis, Optimal design of a novel tuned mass-damper─inerter (TMDI) passive vibration control configuration for stochastically support -excited structural systems. *Probabilistic Engineering Mechanics*, **38**, 156-164, 2014.

[20] C. Málaga-Chuquitaype, C. Menendez-Vicente, R. Thiers-Moggia, Experimental and numerical assessment of the seismic response of steel structures with clutched inerters. *Soil Dynamics and Earthquake Engineering*, **121**, 200-211, 2019.

[21] G. Moghimi, N. Makris, Seismic response of yielding structures equipped with inerters, *Soil Dynamics and Earthquake Engineering*, **141**, 106474, 2021.

[22] N. Makris, M. Aghagholizadeh, Effect of supplemental hysteretic and viscous damping on rocking response of free-standing columns. *Journal of Engineering Mechanics*, **145**(**5**), 04019028, 2019.

[23] M. Aghagholizadeh, N. Makris, Response analysis of yielding structures coupled to rocking walls with supplemental damping. *Earthquake Engineering & Structural Dynamics*, **50**(**10**), 2672-2689, 2021.

[24] R. Thiers-Moggia, C. Málaga-Chuquitaype, Performance-based seismic design and assessment of rocking timber buildings equipped with inerters. *Engineering Structures*, **248**, 113164, 2021.

[25] L. Cao, K.N. Kalfas, N. Makris, J. Ricles, Real-time hybrid simulation of a CLT rocking wall system equipped with pressurized sand dampers for seismic hazard mitigation. *ASCE Engineering Mechanics Institute Conference (EMI2023)*. American Society of Civil Engineers: Atlanta, GA, June 6-9, 2023.

[26] K.N. Kalfas, N. Makris, Estimation of the design parameters of pressurized sand dampers from experiments. *ASCE Engineering Mechanics Institute Conference (EMI2022)*. American Society of Civil Engineers: Baltimore, MD, May 31-June 3, 2022.

[27] U. El Shamy, E. Sabi, K.N. Kalfas, N. Makris, Characterization of energy dissipation during cyclic loading of a sand damper. *ASCE Engineering Mechanics Institute Conference (EMI2022)*. American Society of Civil Engineers: Baltimore, MD, May 31-June 3, 2022.

[28] K.N. Kalfas, N. Makris, Testing of the prototype and sustainable pressurized sand damper for the response modification of structures. *12th US National Conf. on Earthq. Eng.* Earthquake Engineering Research Institute: Salt Lake City, UT, June 27-July 1, 2022.

[29] K.N. Kalfas, *Component testing and characterization of an innovative pressurized sand damper for the response modification of structures*. (Ph.D. Thesis). Southern Methodist University, Dallas, TX, 2023.

[30] K.N. Kalfas, N. Makris, U. El Shamy U, Assessment of the effect of design parameters of pressurized sand dampers from component testing. *Journal of Engineering Mechanics*, **149**(**10**), 04023072, 2023.

[31] M. Karimipetanlar, U. El Shamy, K.N. Kalfas, N. Makris, The influence of particle shape on crushing pattern and energy dissipation within a pressurized sand damper. *Computers & Geotechnics*, **166**, 106020, 2024.

[32] M. Karimipetanlar, U. El Shamy, K.N. Kalfas, N. Makris, Numerical simulations of particle behavior and crushing within a pressurized sand damper subjected to cyclic loading. *Journal of Engineering Mechanics*, **150**(**1**), 04023106, 2024.

[33] K.N. Kalfas, N. Makris, Component testing of cost-effective pressurized sand-dampers. *18th World Conference on Earthquake Engineering (18WCEE)*. International Association of Earthquake Engineering: Milan, IT, June 3-July 5, 2024.

[34] K.N. Kalfas, N. Makris, Component testing of pressurized sand dampers to assess the effect of design parameters. *IABSE Congress San Jose 2024: Beyond Structural Engineering in a Changing World*. International Association for Bridge and Structural Engineering: San Jose, CR, September 25-27, 2024.

[35] K.N. Kalfas, N. Vaiana, N. Makris, A Rate-Independent Phenomenological Model for the Characterization of Pressurized Sand Dampers. *Journal of Engineering Mechanics*, **151**(**4**), 04025007, 2025.

[36] A. Sack, M. Heckel, J.E. Kollmer, F. Zimber, T. Pöschel, Energy dissipation in driven granular matter in the absence of gravity. *Physical Review Letters*, **111**(**1**), 018001, 2013.